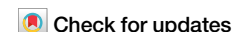




Clinico-physiological correlates of Parkinson's disease from multi-resolution basal ganglia recordings



Srdjan Sumarac ^{1,2}, Jinyoung Youn ^{1,3,4}, Conor Fearon ^{1,3,4}, Luka Zivkovic ^{1,2}, Prerana Keerthi ^{1,2}, Oliver Flouty ^{1,5,6,7}, Milos Popovic ^{2,8,9}, Mojgan Hodaie ^{1,5,6,9}, Suneil Kalia ^{1,6,8,9}, Andres Lozano ^{1,5,6,9}, William Hutchison ^{1,6,9,10}, Alfonso Fasano ^{1,3,4,5,8,9} & Luka Milosevic ^{1,2,5,8,9} ✉

Parkinson's disease (PD) has been associated with pathological neural activity within the basal ganglia. Herein, we analyzed resting-state single-neuron and local field potential (LFP) activities from people with PD who underwent awake deep brain stimulation surgery of the subthalamic nucleus (STN; $n = 125$) or globus pallidus internus (GPi; $n = 44$), and correlated rate-based and oscillatory features with UPDRSIII off-medication subscores. Rate-based single-neuron features did not correlate with PD symptoms. STN single-neuron and LFP low-beta (12–21 Hz) power and burst dynamics showed modest correlations with bradykinesia and rigidity severity, while STN spiketrain theta (4–8 Hz) power correlated modestly with tremor severity. GPi low- and high-beta (21–30 Hz) power and burst dynamics correlated moderately with bradykinesia and axial symptom severity. These findings suggest that elevated single-neuron and LFP oscillations may be linked to symptoms, though modest correlations imply that the pathophysiology of PD may extend beyond resting-state beta oscillations.

Parkinson's disease (PD) is a neurodegenerative disorder characterized by motor symptoms such as bradykinesia, rigidity, and tremor, as well as axial symptoms that affect gait and posture¹. The pathophysiology of PD has been the focal point of numerous studies, leading to significant insights from neurophysiological recordings across various basal ganglia structures². These investigations have not only provided a deeper understanding of the circuit dysfunctions contributing to PD symptoms³, but have also elucidated functional biomarkers that have been instrumental in optimizing targeted therapies like closed-loop deep brain stimulation (DBS), which enables real-time adjustments and a more individualized treatment approach⁴.

The classic "rate" model of PD has been instrumental in describing how alterations in neuronal firing rates relate to the disease^{5–7}. This model attributes the impairment of movement to a series of interconnected neural dysfunctions, particularly an underactivity of the D1-dopamine-receptor-mediated direct pathway medium spiny neurons (dMSN) and overactivity of the D2-mediated indirect pathway medium spiny neurons (iMSN)^{8–10}. Indeed, various studies in preclinical models have shown decreased dMSN

activity and increased iMSN activity^{11–15}, and further downstream, studies have found elevated firing rates in the subthalamic nucleus (STN)^{16–18}, and globus pallidus internus (GPi)^{19–22}, paired with decreased rates in the globus pallidus externus (GPe)^{19,21–25}. However, some evidence from human and non-human primate studies contradicts the classical PD model, showing either significant increases in MSN firing^{26,27}, or no change²⁸, as well as no firing rate change in the substantia nigra pars reticulata (SNr)²⁹. In addition, while dopaminergic agents (such as levodopa) have been shown to decrease GPi firing rate, no significant change was observed in the firing of STN or GPe neurons in response to these agents^{19,21,30}.

A growing body of evidence contends that changes in static firing rates alone do not fully explain the wide spectrum of symptoms in PD. Instead, changes in neuronal firing patterns, such as bursting and over-synchronization of neuronal activity within the basal ganglia play significant roles in PD pathophysiology^{3,31,32}. Numerous studies in both humans and non-human primates indicate changes in bursting activity in the GPi^{21,33–36}, GPe²⁴, and STN¹⁷. Dopamine replacement medication has

¹Krembil Brain Institute, University Health Network, Toronto, ON, Canada. ²Institute of Biomedical Engineering, University of Toronto, Toronto, ON, Canada.

³Edmond J. Safra Program in Parkinson's Disease, Morton and Gloria Shulman Movement Disorders Clinic, Toronto Western Hospital, Toronto, ON, Canada.

⁴Department of Neurology, University of Toronto, Toronto, ON, Canada. ⁵Institute of Medical Sciences, University of Toronto, Toronto, ON, Canada. ⁶Department of Surgery, University of Toronto, Toronto, ON, Canada. ⁷Department of Neurosurgery and Brain Repair, University of South Florida, Tampa, FL, USA. ⁸KITE, University Health Network, Toronto, ON, Canada. ⁹Center for Advancing Neurotechnological Innovation to Application (CRANIA), Toronto, ON, Canada. ¹⁰Department of Physiology, University of Toronto, Toronto, ON, Canada. ✉e-mail: luka.milosevic@mail.utoronto.ca



been found to rectify abnormal neuronal bursting in the striatum³⁰ and pallidum^{19,21}, of non-human primate models of PD, as well as in the human GPi²¹. Additionally, synchronized spike firing within the beta frequency range (15–30 Hz) was first observed in the STN of PD patients undergoing DBS surgery³⁷ and across individual motor cortex neurons in parkinsonian primates³⁸. Research has also shown that tremor-dominant PD patients exhibit prominent oscillations at the tremor frequency (4–8 Hz) within the STN^{39–42}. Despite these findings, establishing the link between synchronized spiking activity and PD has posed significant challenges due to the ephemeral nature of spiking signals and the general scarcity of synchronous firing under physiological conditions⁴³.

Beyond single neuron studies, an examination of local field potentials (LFPs) has significantly advanced our understanding of the neurophysiological mechanisms underlying PD. LFPs represent the aggregate activities of local neuronal populations, including action potential firing, and synaptic currents⁴⁴. Research indicates that elevated beta-band frequencies (13–30 Hz) correlate with the hypokinetic symptoms of PD^{45–54}. However, it is now recognized that the beta activity is divided into two distinct frequency bands, each with unique roles^{55–60}. Oscillations in the low beta (12–21 Hz) range are considered to be pathological and prevalent in untreated PD patients^{54,61,62}. They are more responsive to dopaminergic medication^{45,63,64}, and correlate more closely with disease severity⁵¹. In contrast, high beta has been hypothesized to be related to interregional coupling⁶⁵ and has been linked to the facilitation of motor improvement and force generation^{7,66–68}. While elevated beta power has long been associated with PD, recent investigations emphasize the significance of the temporal dynamics of beta oscillations. Notably, extended periods of heightened beta power (termed ‘beta bursts’), have been associated with bradykinesia and increased reaction times^{69–72}. Treatments like levodopa, electrical stimulation, and neurofeedback training can decrease burst duration and reaction times in people with PD^{69,70,73}. While numerous studies have reported correlations between STN activity and symptom severity in PD^{48,50,53,74}, investigations within the GPi have been far less extensively studied. To the best of our knowledge, only one study has explicitly shown that GPi beta oscillations scale with symptom severity⁷⁵, and a related study has correlated HFO power with bradykinesia during movement⁷⁶. Other studies concerning GPi activity, but not directly related to clinical correlations with motor symptom severity, have been summarized in Supplementary Table 5. Additionally, despite comprehensive LFP research, the intricate relationship between single-neuron oscillatory dynamics and clinical scores has not been studied. This deficiency marks an important avenue for future research, particularly in exploring how spiketrain temporal patterns contribute to the beta bursts characteristic of PD.

In this paper, we interrogate the relationships between PD clinical features and the spectral and temporal characteristics of single-neuron and LFP activities in the STN and GPi of people with PD. We furthermore aimed to address the gap in the literature concerning limited studies directly assessing relationships between clinical and neurophysiological features from single-neuron and LFP features in the GPi. In particular, we leveraged a large database of intracranial recordings acquired during awake DBS surgery of the STN and/or GPi in PD, and assessed rate-based and oscillatory features of spiketrain activity, as well as introduce a new approach to analyze the temporal dynamics of spiketrain oscillations to validate the LFP-derived beta-burst hypothesis at the single-neuron resolution. We moreover perform confirmatory analyses of a similar nature on LFP activity, recorded simultaneously with our single-neuron data, to unify our understanding of clinico-physiological correlates of PD across spatiotemporal neural resolutions⁷⁷.

Results

Single-neuron clinical correlates within the STN

We found no correlations between rate-based neuronal features within the STN (firing rate, burst index, coefficient of variation) and UPDRSIII clinical scores. We observed a slight positive correlation between spiketrain theta power and tremor severity ($\rho = 0.1990$, P value = 0.0260, $BF_{10} = 1.2980$,

BH P value = 0.5610), with anecdotal evidence in favor of the alternative hypothesis. Similarly, we found a slight positive correlation between low beta power and bradykinesia severity ($\rho = 0.2130$, P value = 0.0170, $BF_{10} = 1.8450$, BH P value = 0.5610). Other oscillatory power features did not show any correlations. In terms of temporal burst dynamics of single-neuron activity within the STN, we found slight positive correlations between low beta burst duration and both bradykinesia ($\rho = 0.1760$, P value = 0.0500, $BF_{10} = 0.7500$, BH P value = 0.5610) and rigidity ($\rho = 0.1800$, P value = 0.0440, $BF_{10} = 0.8260$, BH P value = 0.5610), though trends were supported by anecdotal evidence for the null hypothesis. Other oscillatory spiketrain burst dynamic features did not show any correlations. A results summary is displayed in Fig. 1A, with full statistical table found in Supplementary Table 3.

LFP clinical correlates within the STN

We observed a slight positive correlation between low beta LFP power and the total score ($\rho = 0.2790$, P value = 0.0050, $BF_{10} = 6.5540$, BH P value = 0.0550), with moderate evidence in favor of the alternative hypothesis. Additionally, there was a slight positive correlation between low beta LFP power and bradykinesia severity ($\rho = 0.2500$, P value = 0.0110, $BF_{10} = 2.9630$, BH P value = 0.0550), with anecdotal evidence for the alternative hypothesis. For burst dynamics, we found slight positive correlations between low beta LFP mean burst duration and both the total score ($\rho = 0.2520$, P value = 0.0110, $BF_{10} = 3.0990$, BH P value = 0.0550) and bradykinesia severity ($\rho = 0.2550$, P value = 0.0100, $BF_{10} = 3.3900$, BH P value = 0.0550), with moderate evidence for the alternative hypothesis. Other oscillatory LFP burst dynamic features did not show any correlations. A results summary is displayed in Fig. 1B, with the full statistical table found in Supplementary Table 3.

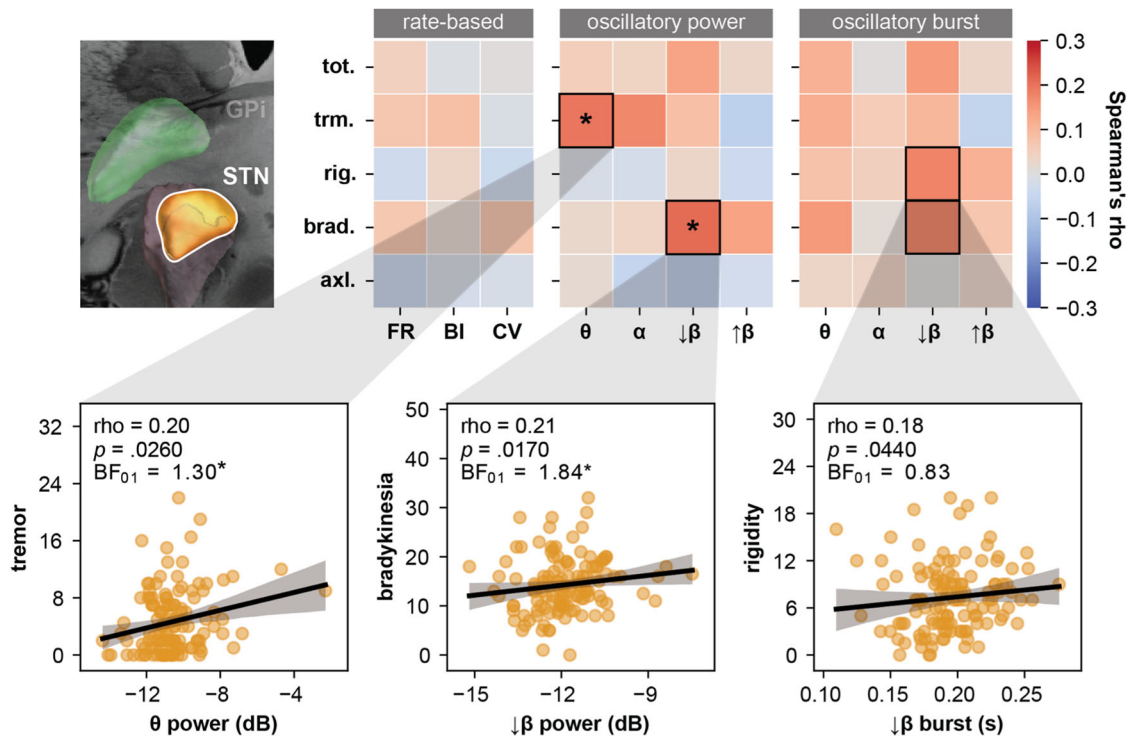
Single-neuron clinical correlates within the GPi

We found no correlations between rate-based neuronal features within the GPi (firing rate, burst index, coefficient of variation) and UPDRSIII clinical scores. We observed a moderate positive correlation between high beta spiketrain power and axial score ($\rho = 0.3890$, P value = 0.0090, $BF_{10} = 5.0640$, BH P value = 0.4950), with moderate evidence in favor of the alternative hypothesis. Moreover, we found slight positive correlations between low beta spiketrain power and both the total score ($\rho = 0.3050$, P value = 0.0440, $BF_{10} = 1.3350$, BH P value = 0.5569) and bradykinesia severity ($\rho = 0.3170$, P value = .0360, $BF_{10} = 1.5700$, BH P value = 0.5569), with anecdotal evidence in favor of the alternative hypothesis. Other oscillatory power features did not show any correlations. In terms of temporal burst dynamics of single-neuron activity within the GPi, we found a slight positive correlation between low beta burst duration and the axial score ($\rho = 0.2830$, P value = 0.0630, $BF_{10} = 1.0020$, BH P value = 0.5569), with anecdotal evidence for the alternative hypothesis. We also found a slight positive correlation between low beta burst duration and bradykinesia ($\rho = 0.2810$, P value = 0.0640, $BF_{10} = 0.9860$, BH P value = 0.5569), though this was supported by anecdotal evidence for the null hypothesis. Other oscillatory spiketrain burst dynamic features did not show any correlations. A results summary is displayed in Fig. 2A, with full statistical table found in Supplementary Table 4. Please note that the GPi rate-based and oscillatory power-based single-neuron correlates with the total UPDRSIII score were also reported in ref. 78.

LFP clinical correlates within the GPi

We observed moderate positive correlations between high beta LFP power and the axial score ($\rho = 0.4640$, P value = 0.0090, $BF_{10} = 6.0470$, BH P value = 0.1600) and low beta LFP power and bradykinesia severity ($\rho = 0.4240$, P value = 0.0180, $BF_{10} = 3.3110$, BH P value = 0.1600), both with moderate evidence in favor of the alternative hypothesis. We also found moderate correlations between low beta LFP power and the axial score ($\rho = 0.4040$, P value = 0.0240, $BF_{10} = 2.5340$, BH P value = 0.1600) and the total score ($\rho = 0.3860$, P value = 0.0320, $BF_{10} = 2.0250$, BH P value = 0.1600), with anecdotal evidence for the alternative hypothesis. For

A spiketrain



B LFP

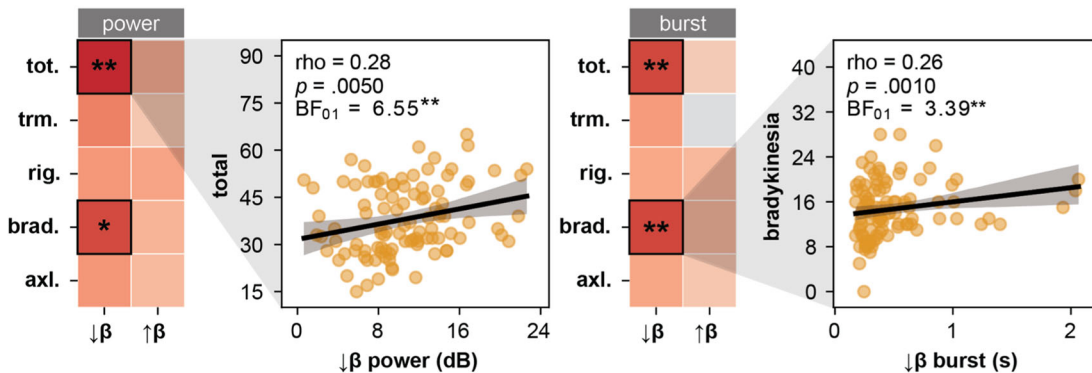


Fig. 1 | STN clinico-physiological correlates. **A** Heatmap shows the Spearman rho correlations of STN spiketrain features (firing rate, burst index, coefficient of variation, oscillatory power and burst dynamics in the theta, alpha, low beta, and high beta frequencies) with clinical scores (total, tremor, rigidity, bradykinesia, and axial UPDRSIII OFF scores). Scatterplots show the top three spiketrain correlations with clinical scores based on the Spearman rho values. **B** Heatmap representing

correlations of low and high beta STN-LFP power and burst dynamics with the aforementioned clinical scores, with scatterplots showing the highest LFP power and burst correlation with clinical scores based on Spearman rho values. Black squares indicate significant correlations (uncorrected for multiple comparisons). Asterisks denote Bayesian evidence in favor of the alternative hypothesis (* anecdotal, ** moderate).

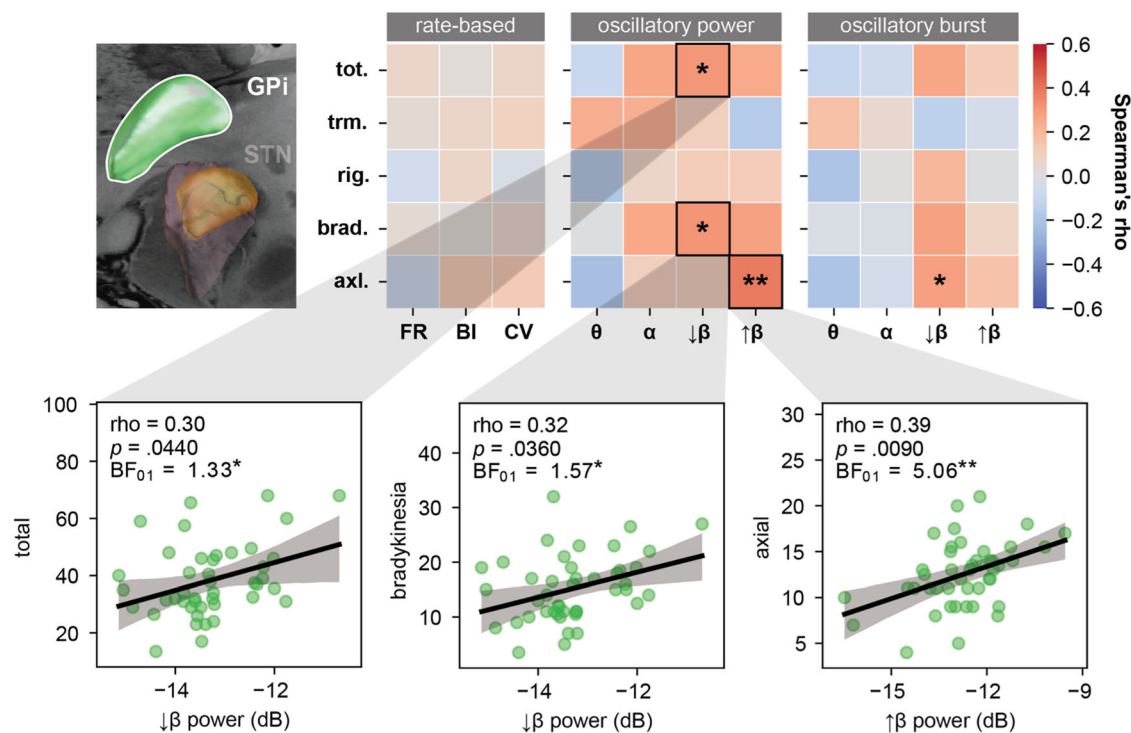
burst dynamics, we found moderate positive correlations between high beta LFP mean burst duration and the axial score ($\rho = 0.3490$, P value = 0.0550, $BF_{10} = 1.3060$, BH P value = 0.1867) and low beta LFP mean burst duration and the axial score ($\rho = 0.3460$, P value = 0.0560, $BF_{10} = 1.2750$, BH P value = 0.1867), both with anecdotal evidence for the alternative hypothesis. Other oscillatory LFP burst dynamic features did not show any correlations. A results summary is displayed in Fig. 2B, with the full statistical table found in Supplementary Table 4.

Discussion

In an effort to better understand the neuronal underpinnings of PD, this study explored the relationships between UPDRSIII OFF subscores and electrophysiological characteristics of the STN and GPi in PD

across a substantial patient cohort. To this end, the significance of uncovering these correlations is twofold. Firstly, they offer deeper insights into the pathophysiology of PD, and may be able to substantiate and/or validate “rate” and “oscillation” model theories of the disorder given the multi-resolution nature of our data (i.e., single-neuron and LFP activities). Secondly, recognizing specific neuronal signatures associated with clinical scores may substantiate existing or motivate novel closed-loop DBS approaches. By placing our findings within the broader academic landscape, we aim to provide a clearer perspective on the relationship between clinical symptoms of PD and their neurobiological counterparts. Noteworthy are the findings related to GPi, which are far sparser in the literature as compared to the myriad of previous LFP studies on STN.

A spiketrain



B LFP

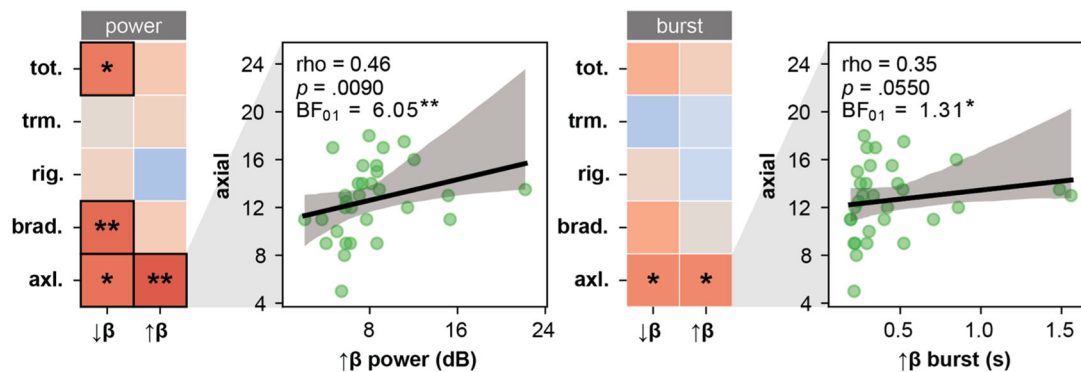


Fig. 2 | GPI clinico-physiological correlates. **A** Heatmap shows the Spearman rho correlations for GPI spiketrain features (firing rate, burst index, coefficient of variation, oscillatory power and burst dynamics across theta, alpha, low beta, and high beta frequencies) with clinical scores (total, tremor, rigidity, bradykinesia, and axial UPDRSIII OFF scores). Scatterplots show the top three spiketrain correlations with clinical scores based on the Spearman rho values. **B** Heatmap shows correlations of

low and high beta GPI LFP power and burst dynamics with the aforementioned clinical scores, with scatterplots showing the highest LFP power and burst correlation with clinical scores based on Spearman rho values. Black squares indicate significant correlations (uncorrected for multiple comparisons). Asterisks denote Bayesian evidence in favor of the alternative hypothesis (* anecdotal, ** moderate).

In our exploration, we did not find any correlations between rate-based metrics (specifically firing rate, burst index, and coefficient of variation) and UPDRSIII OFF clinical subscores in both the STN (Fig. 1A) and GPI (Fig. 2A). This finding challenges the rate and pattern-based models for PD, and is consistent with the broader debate on the classical PD model⁷⁹. Indeed, evidence from 1-Methyl-4-phenyl-1,2,3,6-tetrahydropyridine (MPTP) treated monkeys contradict the classical model, showing inconsistent or unchanged rates post-MPTP despite clinical parkinsonism^{29,80–82}. Moreover, STN DBS at therapeutic frequencies has been shown to increase GPI firing rates in parkinsonian monkeys, despite observations of clinical improvement⁸³. In terms of pattern-based features, though many studies claim parkinsonism significantly alters single-cell firing patterns, evidence suggests that these patterns do not always align with motor impairments in rodent and non-human primate models^{36,82}. Moreover, our recent work in

humans found that neuronal bursting and firing patterns show significant correlations with dystonia symptom severity in the GPI compared with PD, hinting that such patterns might be more characteristic of hyperkinetic disorders than of characteristic hypokinetic features of PD⁷⁸. A plausible explanation for the lack of significance of neuronal firing features is the concept that neurons are capable and have been shown to multiplex^{84,85}. As such, it is possible that the burst patterns observed within the STN or GPI might arise from a superposition of various frequencies at relative timings, which presents as a complex pattern, some of which may not relate to PD. The challenge lies in the overlapping nature of both pathological and physiological signals in these patterns. Without discerning the origin or type of input, attributing these patterns solely to PD becomes difficult. In particular, the burst index may not effectively differentiate between tremor-related spiketrain bursting and beta-related bursting that is thought to

underscore akinetic features of PD. This amalgamation could result in these distinct phenomena being combined, producing a singular, non-specific metric, potentially blurring the relationships with tremor or antikinetic rigid features. As such, analyzing spiketrain oscillations on a frequency-specific basis might bring symptom-specific relationships to light.

Our analysis revealed a slight positive correlation between spiketrain theta oscillatory power and tremor severity in the STN (Fig. 1A). Prior research has shown that PD patients, when off medication, exhibit oscillations at theta frequencies (4–7 Hz) that are synchronized with rest tremor in both the STN^{86–88}, and the GPi⁸⁹. Our analysis builds on these findings by suggesting that theta oscillatory power in the STN also scales with tremor severity; however, this correlation was not evident in the GPi. Additionally, our results align with reports that do not associate tremor with OFF medication beta activity^{90,91}, emphasizing that beta oscillatory activity in the STN may primarily reflect akinetic-rigid symptoms rather than tremor. To this end, our findings show that elevated STN spiketrain and LFP low beta power, as well as prolonged low beta burst slightly correlated with bradykinesia and rigidity (Fig. 1). Previous STN-LFP research has linked beta band power to PD symptoms such as rigidity and bradykinesia^{53,75,92,93}, and abnormal beta bursts were found to correlate with the severity of motor impairments^{69,94}. Interestingly, one study also found that longer burst durations correlated with rigidity-bradykinesia score and shorter bursts correlated with tremor score with the STN⁹⁵. Our work reinforces previous oscillatory PD models and highlights that pathological oscillatory power and temporal dynamics can also be discerned at the single-neuron level^{77,96}.

Our findings also address a knowledge gap in GPi research, which is relatively limited^{97,98}, despite its emerging relevance in discussions on closed-loop GPi-DBS⁹⁹. We found moderate correlations between low beta power and bradykinesia, as well as surprising correlations between high beta activity and axial scores (Fig. 2). This could suggest unique neural mechanisms in the GPi that may be important for PD-specific manifestations like gait and balance dysfunction. Indeed, the high beta (21–35 Hz) band, previously tied to interregional coupling, possibly aids motor enhancement and force generation^{66–68}. However, the connection between axial symptoms and high beta oscillations in the GPi remains largely unexplored, with one similar GPi LFP study not showing any correlations with axial symptoms⁷⁵. One study observed that high beta activity was more prominent in patients with postural instability and gait disorder (PIGD) compared to those with a tremor-dominant presentation, specifically within the STN¹⁰⁰. Our findings may extend this observation to the GPi, indicating that high beta oscillations within this region could also be associated with PIGD symptoms in PD. The absence of notable oscillatory burst-related findings in the GPi may be attributed to its complex role within the basal ganglia network, where the manifestations of burst dynamics do not parallel those observed in the STN, possibly due to differences in their neurophysiological responses to PD pathology.

When comparing our findings on single-neuron dynamics to those from LFP studies, we observed that burst durations were much shorter in spiketrain data. The difference is likely due to the higher spatiotemporal resolution of single-neuron activity compared to LFPs. Our group has previously demonstrated that single-neuron bursts within the STN typically precede LFP oscillations, suggesting that synchronous neuronal bursting within the STN gives rise to aggregate-level LFP oscillations in PD⁷⁷. Therefore, while individual neurons may transition in and out of their pathological bursting phases at fast time courses, these transitions are likely to be blurred when averaged across aggregate populations, resulting in longer burst episodes seen in LFPs. Another possible explanation is that LFPs represent not only the summed electrical activity from a population of neurons but also synaptic potentials and other subthreshold activities that do not necessarily result in spike output^{43,101}, which could also contribute to burst generation.

The correlations reported in this work were relatively modest, suggesting that while elevated resting-state beta activity is linked to symptoms, it might not fully explain the complex neuronal mechanisms underlying PD. Indeed, beta oscillations in the basal ganglia are not unequivocally considered as pathological, as evidenced by non-human primate studies¹⁰², and implicated roles in cognition¹⁰³. In fact, several studies have shown that

~25% of patients did not exhibit pronounced beta activity even though they experienced symptoms^{100,104,105}.

While our analyses generally highlight convergence in findings between STN and GPi related to low beta power, some notable differences were also identified, potentially emphasizing different roles in basal ganglia circuitry and PD pathophysiology. One such difference is that that single neuron oscillatory power within the STN appeared to be more closely linked with tremor compared to the GPi (Figs. 1A and 2A). Research has shown that while both STN and GPi-DBS effectively suppress tremor, STN DBS offers quicker initial action tremor improvement, though this advantage diminishes over time compared to GPi-DBS¹⁰⁶. Moreover, research pertaining to the modulation of axial symptoms such as postural instability and gait impairment, may spark debate when comparing the efficacy of GPi-DBS and STN DBS. Some studies indicate STN DBS offers better relief from axial symptoms than GPi-DBS¹⁰⁷, while others find no significant difference in gait and axial UPDRS scores when medications are not in play between the two¹⁰⁸. However, a meta-regression study suggests that GPi-DBS may in fact be more effective in preserving axial symptoms over time^{109,110}. Still, the decline in axial abilities post-DBS can be attributed to multiple factors, including (but not limited to) disease progression and medication adjustments¹¹⁰. Understanding the relationship between single-neuron dynamics, oscillatory patterns, and PD symptoms may perhaps enhance our grasp on the effectiveness of GPi vs. STN DBS in managing specific symptoms.

A limitation inherent to our intraoperative studies in humans is the absence of healthy control data, which hampers our ability to establish normative baselines. Additionally, the granular details regarding the depth of recorded neurons were not documented in our current dataset, potentially obscuring finer nuances in our findings. Moreover, LFP analyses were limited to beta frequency oscillations, given the frequent use of a 10 Hz hardware one-pole high pass filter in the intraoperative environment, which within the context of this work, we were not able to retroactively control for. However, past studies show that LFP in the motor cortico-basal ganglia circuit do not reflect tremor oscillations as distinctly as single neuron recordings¹¹¹. Moreover, while we have removed spiking templates from LFP signals, contamination of spiking activity cannot be entirely ruled out. However, some authors suggest that the LFP predominantly results from subthreshold membrane dynamics rather than spiking activity^{43,101}, and that lower frequency (i.e. beta) contamination is considered minimal¹¹², and thus can be considered as distinct metrics. Additionally, it has been reported that burst duration and power in LFP signals may provide equivalent information if corresponding measures are used¹¹³, although we report these as separate metrics as other authors have^{50,69,70}. Given the potential overlap in various metrics for assessing oscillatory dynamics, we have also considered a consolidated approach in generating an amalgamated oscillatory metric (see Supplementary Fig. 2 and Supplementary Tables 6 and 7 for statistics). The inability to use pharmacological agents during our intraoperative human studies also poses a constraint. Such agents, in controlled settings, could offer deeper insights into the mechanistic aspects of identified neural interactions. Due to the extensive number of tests conducted, none of our correlations remain significant after adjusting for multiple comparisons, warranting cautious interpretation of the results. Finally, while our use of microelectrodes affords higher spatial resolution, it may capture a more limited LFP spatial domain than traditional DBS macroelectrode recordings. A final potential confounder of our dataset in particular is that the motor symptom assessments were not conducted concurrently with the microelectrode recording, but were conducted at a pre-surgical timepoint (~35 weeks), which may be associated to potential variations in in-real-time symptom presentation.

Our research elucidates the clinical and physiological links between oscillatory characteristics and PD symptoms, demonstrating these associations at various spatiotemporal scales within the STN and the GPi. In the STN, enhanced low-beta oscillations and prolonged burst durations were associated with bradykinesia and rigidity, while the amplitude of spiketrain theta oscillation correlated with tremor severity. Moreover, our findings also show that the strength of low-beta oscillations in the GPi is associated with bradykinesia, while high-beta oscillations correlate with axial symptoms.

Our findings generally underscore the important role of neuronal oscillations in PD pathophysiology. However, the modest correlations also suggest that the complexity of PD may extend beyond beta oscillations alone, indicating that other neural dynamics may contribute to the clinical manifestations of PD.

Methods

Patient demographics and clinical data

We conducted offline analyses of resting-state intraoperative electrophysiological data collected from people with PD (43 female; 126 male) undergoing awake microelectrode-guided placement of DBS electrodes in STN ($n = 125$) or GPi ($n = 44$) after 12-h withdrawal from antiparkinsonian medications. The average age at the time of surgery was 60.9 ± 7.5 years, with an average disease duration of 11.1 ± 4.5 years. Pre-operative clinical scores of motor symptom severity in the OFF-medication states were obtained using the Unified Parkinson's Disease Rating Score Part III (UPDRSIII), and decomposed into several subscores, including tremor (sum of items 20–21, assessing kinetic and rest tremor), rigidity (item 22, assessing neck and limb stiffness), bradykinesia (items 23–26, assessing slowness of movement), and axial symptoms (items 27–31, assessing gait and posture), in addition to total motor score (items 18–31). Individual patient data is available in Supplementary Table 1. A statistics summary of demographic and clinical data is provided in Supplementary Table 2. Our study conformed to the guidelines provided by the Tri-Council Policy on Ethical Conduct for Research Involving Humans. All procedures were subject to approval by the University Health Network Research Ethics Board, and each patient gave informed written consent.

Surgery and microelectrode recording procedure

The electrophysiological identification of the STN and the GPi was performed utilizing previously published methods¹¹⁴. Briefly, the anterior commissure (AC) and posterior commissure (PC) stereotactic coordinates were identified through pre-operative T1 and T2 magnetic resonance images (Signa, 3 T). The positions of the STN or the GPi were estimated based on these coordinates, in conjunction with the Schaltenbrand and Wahren stereotactic brain atlas (1977). We employed commercial planning software (Stealth Workstation, Medtronic) to carry out direct visualization of the target and the trajectory of approach on T1–T2 fused images. Subsequently, a custom microelectrode recording (MER) setup comprised of two microelectrodes (600 μm apart, 0.1–0.4 M Ω impedances) which shared a common ground on a stainless-steel intracranial guide tube were independently advanced in the brain beginning 10 mm above the MRI-planned target. Upon confirmation of the targeted brain structure, the recordings were amplified using either the GS3000 Guideline System (Axon Instruments) or the Guideline 4000 LP+ (FHC) and digitized at a rate of ≥ 10 kHz using a CED1401 data acquisition system (Cambridge Electronic Design). The data was then stored for offline analysis, with no interim analysis performed prior to full data collection. Instead, each MER was visually inspected for resting state neuronal segments, and only neurons that strictly adhered to pre-defined quality metrics (see section below) were considered for analysis.

Offline analysis of single-neuron activity

The single-neuron database included 938 MER segments from the STN and 222 segments from the GPi, which were ≥ 5 s in duration. For the single-neuron analysis, we built a custom Python-based graphical user interface to process each MER segment. The software, along with its instructions and documentation, is available for download at <https://github.com/Toronto-TNBS/spooky-spikes>. Briefly, MER segments were bandpass filtered (300–3000 Hz) using a 4th-order Butterworth filter with zero-phase distortion. Then, the spike detection threshold was set using a multiple of an estimate of the standard deviation of the noise¹¹⁵, and each detected spike was extracted and sorted using K-means clustering with silhouette scoring to determine the optimal number of clusters (see Supplementary Material for software details). Only neurons sufficiently isolated with a signal-to-noise ratio exceeding 4, and those demonstrating less than 1% interspike

interval violations were included. Subsequently, a variety of spiketrain features were extracted from each MER segment. These included the median firing rate, burst index, coefficient of variation, spike-train oscillatory power, and average oscillatory burst duration across different frequency bands: theta (4–8 Hz), alpha (8–12 Hz), low beta (12–21 Hz), and high beta (21–30 Hz). The firing rate was calculated as the inverse of the mean interspike interval distribution (Fig. 3A). The burst index was calculated using the ratio of means from a two-component Gaussian mixture model applied to the log interspike interval distribution, a modified approach to the traditional mode-over-mean interspike interval (ISI) method (Fig. 3A)³³. The robust coefficient of variation was determined by dividing the median absolute deviation of the interspike interval distribution by its median, adopting a modified approach from the previously used standard deviation over mean ISI method (Fig. 3A)¹¹⁶. Oscillatory power was extracted using Lomb's periodogram, conducted on the autocorrelation function of single-neuron segments, as previously described¹¹⁷ (Fig. 3B). We deployed a novel oscillatory burst detection algorithm to ascertain the duration of time a neuron spent spontaneously bursting within a specific frequency range (Fig. 3C). Briefly, the spiketrain of a neuron was first converted into a binary sequence and then downsampled to 500 Hz. Subsequently, we filtered the binary sequence into the frequency band of interest, ranging from theta to high beta using a 4th order zero-phase Butterworth filter, thus converting the spiketrain into an LFP-like signal. For burst determination, we adopted a novel method that classifies burst durations when oscillatory activity surpasses the overall noise floor within a recording, as employed in ref. 118. This involved enveloping the filtered binary sequence in each frequency band using the absolute value of the Hilbert transform. An oscillatory burst was then identified when its amplitude surpassed a threshold for more than 100 ms, defined as four times the median of averaged peaks from envelopes of five overlapping 6 Hz bands in the low gamma band (45–55 Hz) from the same MER segment. We determined the gamma waveforms using the filtered binary sequence approach. We then extracted the average burst duration which is the time spent above the determined threshold.

Offline analysis of LFP

We analysed the LFP power in both low and high beta frequency ranges from a subset of MER segments that were used in the single-neuron analysis. This subset comprised of 572 MER segments from the STN ($n = 102$), and 135 MER segments from the GPi ($n = 31$). A subset was necessary because some MER recordings had hardware one-pole high-pass filters of >250 Hz, which precluded LFP analysis. In addition, segments possessing either multi-unit activity or unfilterable artifacts (typically large cardiac artifacts) were omitted from the analysis to prevent contamination of the LFP data. First, we employed the spike-removal technique described in ref. 119, which involves interpolating neural spikes with random segments representative of general noise in the signal. Then, after spike removal, each MER segment was low-pass filtered using a 4th order zero-phase Butterworth filter, then downsampled to 250 Hz and z-score normalized. Subsequently, Welch's method was applied with the number of samples per segment set to 256. Each power spectral density was further normalized to the sum of frequencies spanning 45–55 Hz. Since our MER data were subjected to a 10 Hz hardware one-pole high pass filter, we extracted only low- (12–21 Hz) and high- (21–30 Hz) beta powers by calculating the sum of the power in these respective frequency ranges. For burst determination, we utilized a method that classifies beta bursts when beta activity surpasses the overall noise floor within a recording, as previously employed^{50,118,120}. Briefly, the raw signal was bandpass-filtered around the frequency band of interest (either low or high beta band) using a 4th order zero-phase Butterworth filter and envelope peaks were calculated using the absolute value of the Hilbert transform. A beta burst was identified when the amplitude exceeded a threshold for more than 100 ms, and defined as four times the median of averaged peaks from envelopes of five overlapping 6 Hz bands in the low gamma band (45–55 Hz) from the same MER segment. From the analysis, we extracted LFP power and burst duration in the low beta and high beta frequency bands (see Fig. 4 for details).

Fig. 3 | Analysis of single-neuron activity from microelectrode recordings. **A** A 5-second example trace illustrates a neuron firing in an irregular pattern. The panel beneath displays the log interspike interval of the spiketrain, with a double Gaussian exponential fit applied to quantify the neuron's firing patterns. **B** Four example traces represent neurons oscillating within the theta, alpha, low beta, and high beta frequency ranges over a 1-s duration. For each frequency, the corresponding spiketrain autocorrelation functions span a half-second lag. The Lomb-Scargle periodogram of the autocorrelation function is also provided, helping to quantify the strength of the neuronal oscillation. **C** An example trace demonstrates a neuron exhibiting strong low beta oscillations. Below this, the downsampled binary sequence of the spiketrain is displayed as a gray trace. The green wave represents the low beta filtered binary sequence, and the black trace illustrates the Hilbert-transformed waveform of the beta power amplitude. The horizontal orange line indicates the burst duration threshold, while the red boxes pinpoint detected bursts.

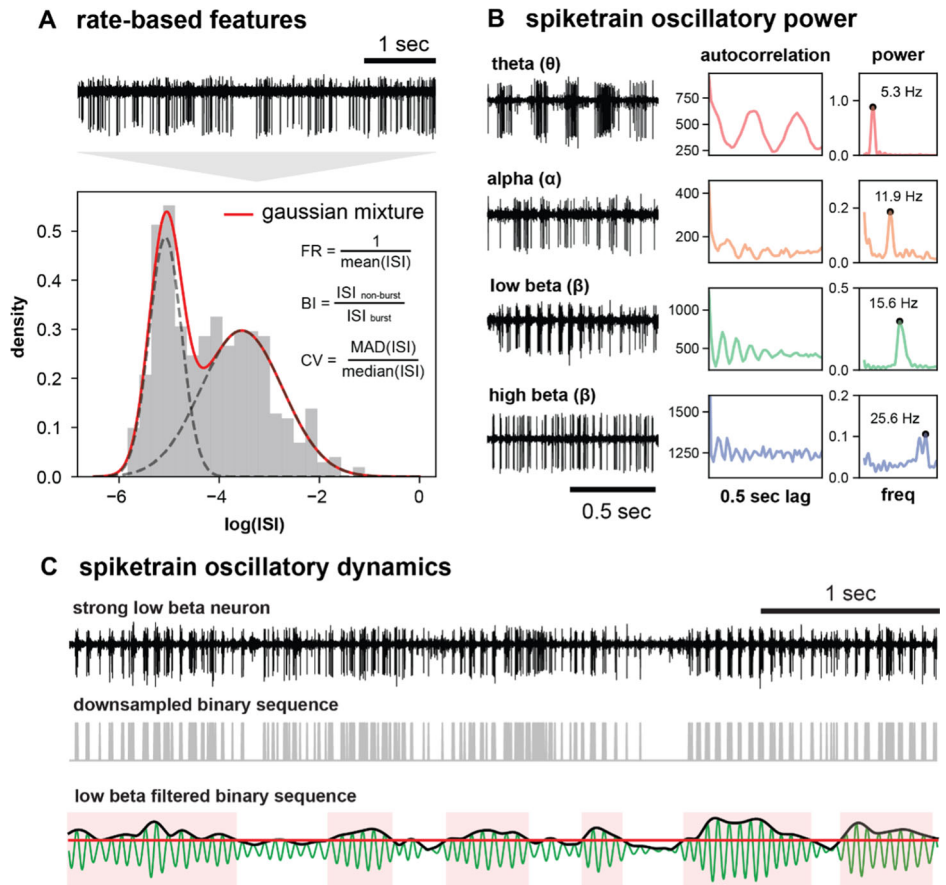
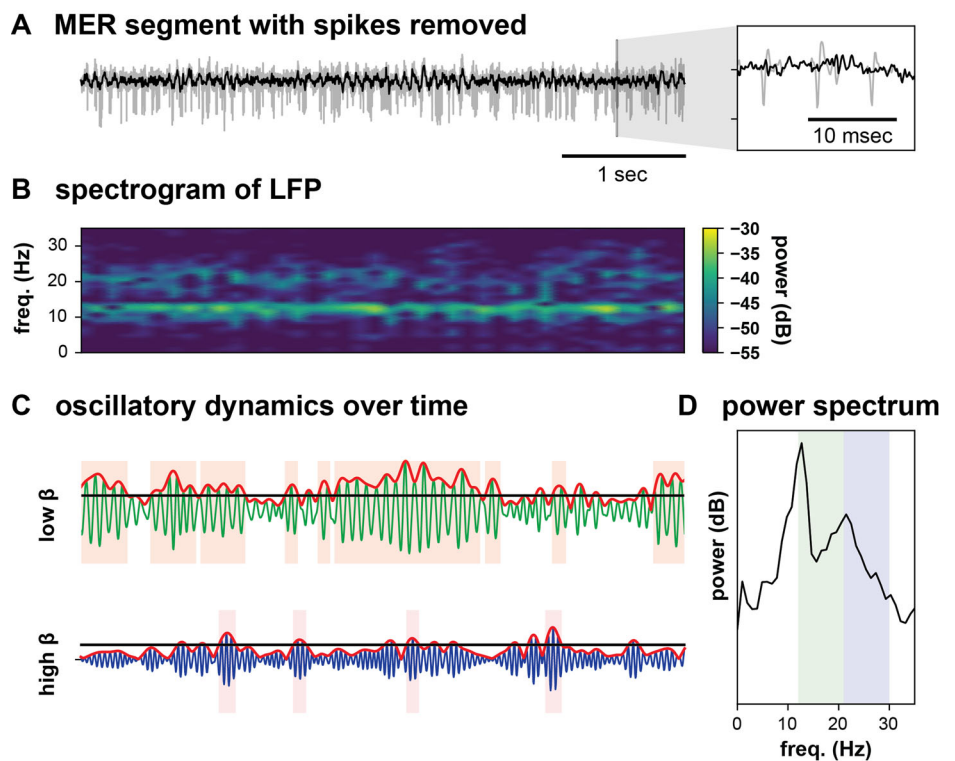


Fig. 4 | Analysis of LFP activity from microelectrode recordings. **A** The example trace illustrates a downsampled 5 s MER segment with spikes removed emphasizing only the LFP. **B** Shows the spectrogram of the MER segment. **C** Shows the oscillatory dynamic of LFP power, with the green wave representing the low beta filtered MER signal, the blue wave represents the high beta filtered signal, and the red traces depict the Hilbert-transformed waveforms of the beta power amplitudes. The horizontal black line marks the burst duration threshold, and the red boxes highlight detected bursts. **D** Shows the power spectral density of the MER segment in the decibel scale.



Statistical analyses

All statistical analyses were conducted in JASP (version 0.18.3). Briefly, we performed Spearman correlations between each combination of UPDRSIII clinical scores (total, bradykinesia, rigidity, tremor, axial) and neural features. The single-neuron features included the median firing rate for each patient, as well as the 90th percentile of burst index, coefficient of variation, oscillatory powers (theta, alpha, low beta, and high beta), and mean burst durations (theta, alpha, low beta, and high beta) per patient. The LFP features included the 90th percentile for both low and high beta power and their respective average burst durations. We applied the Benjamini-Hochberg (BH) method to control for false discovery rates in multiple comparisons, with the results provided in Supplementary Tables 3 and 4. In addition to frequentist statistics, we employed Bayesian Spearman correlations to evaluate the evidence for the presence (alternative hypothesis) or absence (null hypothesis) of correlations. Since JASP does not natively support Bayesian Spearman correlations, we first ranked all features and then applied Pearson's *r* to these ranked variables to effectively perform the Bayesian Spearman correlations using the default prior.

Data availability

The datasets used and/or analysed during the current study available from the corresponding author on reasonable request.

Code availability

The underlying code for this study is available in the Toronto-TNBS/spooky-spikes repository and can be accessed via this link <https://github.com/Toronto-TNBS/spooky-spikes>.

Received: 6 January 2024; Accepted: 5 August 2024;

Published online: 12 September 2024

References

- Jankovic, J. Parkinson's disease: clinical features and diagnosis. *J. Neurol. Neurosurg. Psychiatry* **79**, 368–376 (2008).
- Chen, R. et al. Clinical neurophysiology of Parkinson's disease and parkinsonism. *Clin. Neurophysiol. Pract.* **7**, 201–227 (2022).
- McGregor, M. M. & Nelson, A. B. Circuit mechanisms of Parkinson's disease. *Neuron* **101**, 1042–1056 (2019).
- Bouthour, W. et al. Biomarkers for closed-loop deep brain stimulation in Parkinson disease and beyond. *Nat. Rev. Neurol.* **15**, 343–352 (2019).
- Albin, R. L., Young, A. B. & Penney, J. B. The functional anatomy of basal ganglia disorders. *Trends Neurosci.* **12**, 366–375 (1989).
- DeLong, M. R. Primate models of movement disorders of basal ganglia origin. *Trends Neurosci.* **13**, 281–285 (1990).
- Alexander, G. E. & Crutcher, M. D. Functional architecture of basal ganglia circuits: neural substrates of parallel processing. *Trends Neurosci.* **13**, 266–271 (1990).
- Deng, Y.-P., Lei, W.-L. & Reiner, A. Differential perikaryal localization in rats of D1 and D2 dopamine receptors on striatal projection neuron types identified by retrograde labeling. *J. Chem. Neuroanat.* **32**, 101–116 (2006).
- Gerfen, C. R. et al. D1 and D2 dopamine receptor-regulated gene expression of striatonigral and striatopallidal neurons. *Science* **250**, 1429–1432 (1990).
- Herve, D., Rogard, M. & Le'vi-Strauss, M. Molecular analysis of the multiple Golf α subunit mRNAs in the rat brain. *Mol. Brain Res.* **32**, 125–134 (1995).
- Kita, H. & Kita, T. Role of striatum in the pause and burst generation in the globus pallidus of 6-OHDA-treated rats. *Front. Syst. Neurosci.* **5**, 42 (2011).
- Sagot, B., Li, L. & Zhou, F.-M. Hyperactive response of direct pathway striatal projection neurons to L-dopa and D1 agonism in freely moving Parkinsonian mice. *Front. Neural Circ.* **12**, 57 (2018).
- Ryan, M. B., Bair-Marshall, C. & Nelson, A. B. Aberrant striatal activity in parkinsonism and levodopa-induced dyskinesia. *Cell Rep.* **23**, 3438–3446.e5 (2018).
- Parker, J. G. et al. Diametric neural ensemble dynamics in parkinsonian and dyskinesic states. *Nature* **557**, Art. no. 7704 (2018).
- Mallet, N. et al. Dichotomous organization of the external globus pallidus. *Neuron* **74**, 1075–1086 (2012).
- Benazzouz, A. et al. Intraoperative microrecordings of the subthalamic nucleus in Parkinson's disease. *Mov. Disord.* **17**, S145–S149 (2002).
- Bergman, H., Wichmann, T., Karmon, B. & DeLong, M. R. The primate subthalamic nucleus. II. Neuronal activity in the MPTP model of parkinsonism. *J. Neurophysiol.* **72**, 507–520 (1994).
- Kreiss, D. S., Mastropietro, C. W., Rawji, S. S. & Walters, J. R. The response of subthalamic nucleus neurons to dopamine receptor stimulation in a rodent model of Parkinson's disease. *J. Neurosci.* **17**, 6807–6819 (1997).
- Filion, M. & Tremblay, L. Abnormal spontaneous activity of globus pallidus neurons in monkeys with MPTP-induced parkinsonism. *Brain Res.* **547**, 142–151 (1991).
- Boraud, T., Bezard, E., Bioulac, B. & Gross, C. High frequency stimulation of the internal Globus Pallidus (GPI) simultaneously improves parkinsonian symptoms and reduces the firing frequency of GPI neurons in the MPTP-treated monkey. *Neurosci. Lett.* **215**, 17–20 (1996).
- Boraud, T., Bezard, E., Guehl, D., Bioulac, B. & Gross, C. Effects of L-DOPA on neuronal activity of the globus pallidus externalis (GPe) and globus pallidus internalis (GPI) in the MPTP-treated monkey. *Brain Res.* **787**, 157–160 (1998).
- Heimer, G., Bar-Gad, I., Goldberg, J. A. & Bergman, H. Dopamine replacement therapy reverses abnormal synchronization of pallidal neurons in the 1-methyl-4-phenyl-1,2,3,6-tetrahydropyridine primate model of parkinsonism. *J. Neurosci.* **22**, 7850–7855 (2002).
- Pan, H. S. & Walters, J. R. Unilateral lesion of the nigrostriatal pathway decreases the firing rate and alters the firing pattern of globus pallidus neurons in the rat. *Synapse* **2**, 650–656 (1988).
- Soares, J. et al. Role of external pallidal segment in primate parkinsonism: comparison of the effects of 1-methyl-4-phenyl-1,2,3,6-tetrahydropyridine-induced parkinsonism and lesions of the external pallidal segment. *J. Neurosci.* **24**, 6417–6426 (2004).
- Mallet, N. et al. Parkinsonian beta oscillations in the external globus pallidus and their relationship with subthalamic nucleus activity. *J. Neurosci.* **28**, 14245–14258 (2008).
- Liang, L., DeLong, M. R. & Papa, S. M. Inversion of dopamine responses in striatal medium spiny neurons and involuntary movements. *J. Neurosci.* **28**, 7537–7547 (2008).
- Singh, A. et al. Human striatal recordings reveal abnormal discharge of projection neurons in Parkinson's disease. *Proc. Natl. Acad. Sci. USA.* **113**, 9629–9634 (2016).
- Deffains, M. et al. Subthalamic, not striatal, activity correlates with basal ganglia downstream activity in normal and Parkinsonian monkeys. *eLife* **5**, e16443 (2016).
- Wichmann, T. et al. Comparison of MPTP-induced changes in spontaneous neuronal discharge in the internal pallidal segment and in the substantia nigra pars reticulata in primates. *Exp. Brain Res.* **125**, 397–409 (1999).
- Levy, R. et al. Lidocaine and muscimol microinjections in subthalamic nucleus reverse Parkinsonian symptoms. *Brain J. Neurol.* **124**, 2105–2118 (2001).
- Bevan, M. D., Magill, P. J., Terman, D., Bolam, J. P. & Wilson, C. J. Move to the rhythm: oscillations in the subthalamic nucleus-external globus pallidus network. *Trends Neurosci* **25**, 525–531 (2002).
- Nini, A., Feingold, A., Sloviter, H. & Bergman, H. Neurons in the globus pallidus do not show correlated activity in the normal monkey, but

- phase-locked oscillations appear in the MPTP model of parkinsonism. *J. Neurophysiol.* **74**, 1800–1805 (1995).
33. Hutchison, W. D. et al. Differential neuronal activity in segments of globus pallidus in Parkinson's disease patients. *Neuroreport* **5**, 1533–1537 (1994).
 34. Starr, P. A. et al. Spontaneous pallidal neuronal activity in human dystonia: comparison with Parkinson's disease and normal macaque. *J. Neurophysiol.* **93**, 3165–3176 (2005).
 35. Miller, W. C. & DeLong, M. R. Parkinsonian symptomatology. An anatomical and physiological analysis. *Ann. N. Y. Acad. Sci.* **515**, 287–302 (1988).
 36. Muralidharan, A. et al. Physiological changes in the pallidum in a progressive model of Parkinson's disease: are oscillations enough? *Exp. Neurol.* **279**, 187–196 (2016).
 37. Levy, R., Hutchison, W. D., Lozano, A. M. & Dostrovsky, J. O. High-frequency synchronization of neuronal activity in the subthalamic nucleus of parkinsonian patients with limb tremor. *J. Neurosci.* **20**, 7766–7775 (2000).
 38. Goldberg, J. A. et al. Enhanced synchrony among primary motor cortex neurons in the 1-methyl-4-phenyl-1,2,3,6-tetrahydropyridine primate model of Parkinson's disease. *J. Neurosci.* **22**, 4639–4653 (2002).
 39. Hirschmann, J. et al. Parkinsonian rest tremor is associated with modulations of subthalamic high-frequency oscillations. *Mov. Disord.* **31**, 1551–1559 (2016).
 40. Reck, C. et al. Coherence analysis of local field potentials in the subthalamic nucleus: differences in parkinsonian rest and postural tremor. *Eur. J. Neurosci.* **32**, 1202–1214 (2010).
 41. Timmermann, L. et al. The cerebral oscillatory network of parkinsonian resting tremor. *Brain J. Neurol.* **126**, 199–212 (2003).
 42. Reck, C. et al. Characterisation of tremor-associated local field potentials in the subthalamic nucleus in Parkinson's disease. *Eur. J. Neurosci.* **29**, 599–612 (2009).
 43. Buzsáki, G., Anastassiou, C. A. & Koch, C. The origin of extracellular fields and currents—EEG, ECoG, LFP and spikes. *Nat. Rev. Neurosci.* **13**, 407–420 (2012).
 44. Yin, Z. et al. Local field potentials in Parkinson's disease: a frequency-based review. *Neurobiol. Dis.* **155**, 105372 (2021).
 45. Brown, P. et al. Dopamine dependency of oscillations between subthalamic nucleus and pallidum in Parkinson's disease. *J. Neurosci.* **21**, 1033–1038 (2001).
 46. Canessa, A. et al. Striatal dopaminergic innervation regulates subthalamic beta-oscillations and cortical-subcortical coupling during movements: preliminary evidence in subjects with Parkinson's disease. *Front. Hum. Neurosci.* **10**, 611 (2016).
 47. Joundi, R. A. et al. Persistent suppression of subthalamic beta-band activity during rhythmic finger tapping in Parkinson's disease. *Clin. Neurophysiol.* **124**, 565–573 (2013).
 48. Kühn, A. A. et al. Event-related beta desynchronization in human subthalamic nucleus correlates with motor performance. *Brain J. Neurol.* **127**, 735–746 (2004).
 49. Litvak, V. et al. Movement-related changes in local and long-range synchronization in Parkinson's disease revealed by simultaneous magnetoencephalography and intracranial recordings. *J. Neurosci.* **32**, 10541–10553 (2012).
 50. Lofredi, R. et al. Subthalamic beta bursts correlate with dopamine-dependent motor symptoms in 106 Parkinson's patients. *NPJ Parkinson's Dis.* **9**, 2 (2023).
 51. Neumann, W.-J. et al. Subthalamic synchronized oscillatory activity correlates with motor impairment in patients with Parkinson's disease. *Mov. Disord.* **31**, 1748–1751 (2016).
 52. Brittain, J. S. & Brown, P. Oscillations and the basal ganglia: motor control and beyond. *Neuroimage* **85**, 637–647 (2014).
 53. Kühn, A. A. et al. Pathological synchronisation in the subthalamic nucleus of patients with Parkinson's disease relates to both bradykinesia and rigidity. *Exp. Neurol.* **215**, 380–387 (2009).
 54. Oswal, A. et al. Deep brain stimulation modulates synchrony within spatially and spectrally distinct resting state networks in Parkinson's disease. *Brain J. Neurol.* **139**, 1482–1496 (2016).
 55. Hirschmann, J. et al. Longitudinal recordings reveal transient increase of alpha/low-beta power in the subthalamic nucleus associated with the onset of Parkinsonian rest tremor. *Front. Neurol.* **10**, 145 (2019).
 56. Kato, K. et al. Bilateral coherence between motor cortices and subthalamic nuclei in patients with Parkinson's disease. *Clin. Neurophysiol.* **126**, 1941–1950 (2015).
 57. Little, S., Pogosyan, A., Kuhn, A. A. & Brown, P. band stability over time correlates with Parkinsonian rigidity and bradykinesia. *Exp. Neurol.* **236**, 383–388 (2012).
 58. Litvak, V. et al. Resting oscillatory cortico-subthalamic connectivity in patients with Parkinson's disease. *Brain J. Neurol.* **134**, 359–374 (2011).
 59. Oswal, A., Brown, P. & Litvak, V. Synchronized neural oscillations and the pathophysiology of Parkinson's disease. *Curr. Opin. Neurol.* **26**, 662 (2013).
 60. van Wijk, B. C. M. et al. Subthalamic nucleus phase-amplitude coupling correlates with motor impairment in Parkinson's disease. *Clin. Neurophysiol.* **127**, 2010–2019 (2016).
 61. Tsiokos, C., Malekmohammadi, M., AuYong, N. & Pouratian, N. Pallidal low β -low γ phase-amplitude coupling inversely correlates with Parkinson disease symptoms. *Clin. Neurophysiol.* **128**, 2165–2178 (2017).
 62. López-Azcárate, J. et al. Coupling between beta and high-frequency activity in the human subthalamic nucleus may be a pathophysiological mechanism in Parkinson's disease. *J. Neurosci.* **30**, 6667–6677 (2010).
 63. Whitmer, D. et al. High frequency deep brain stimulation attenuates subthalamic and cortical rhythms in Parkinson's disease. *Front. Hum. Neurosci.* **6**, 155 (2012).
 64. Eusebio, A. et al. Deep brain stimulation can suppress pathological synchronisation in Parkinsonian patients. *J. Neurol. Neurosurg. Psychiatry* **82**, 569–573 (2011).
 65. Oswal, A. et al. Neural signatures of hyperdirect pathway activity in Parkinson's disease. *Nat. Commun.* **12**, 5185 (2021).
 66. Florin, E. et al. Does increased gamma activity in patients suffering from Parkinson's disease counteract the movement inhibiting beta activity? *Neuroscience* **237**, 42–50 (2013).
 67. Ozturk, M. et al. Distinct subthalamic coupling in the ON state describes motor performance in Parkinson's disease. *Mov. Disord.* **35**, 91–100 (2020).
 68. Blumenfeld, Z. et al. Sixty-hertz stimulation improves bradykinesia and amplifies subthalamic low-frequency oscillations. *Mov. Disord.* **32**, 80–88 (2017).
 69. Tinkhauser, G. et al. Beta burst dynamics in Parkinson's disease OFF and ON dopaminergic medication. *Brain J. Neurol.* **140**, 2968–2981 (2017).
 70. Lofredi, R. et al. Beta bursts during continuous movements accompany the velocity decrement in Parkinson's disease patients. *Neurobiol. Dis.* **127**, 462–471 (2019).
 71. Shin, H., Law, R., Tsutsui, S., Moore, C. I. & Jones, S. R. The rate of transient beta frequency events predicts behavior across tasks and species. *eLife* **6**, e29086 (2017).
 72. Torrecillos, F. et al. Modulation of beta bursts in the subthalamic nucleus predicts motor performance. *J. Neurosci.* **38**, 8905–8917 (2018).
 73. He, S., Everest-Phillips, C., Clouter, A., Brown, P. & Tan, H. Neurofeedback linked suppression of cortical β bursts speeds up

- movement initiation in healthy motor control: a double-blind sham-controlled study. *J. Neurosci.* **40**, 4021–4032 (2020).
74. Morelli, N. & Summers, R. L. S. Association of subthalamic beta frequency sub-bands to symptom severity in patients with Parkinson's disease: a systematic review. *Parkinsonism Relat. Disord.* **110**, 105364 (2023).
 75. Eisinger, R. S. et al. Parkinsonian beta dynamics during rest and movement in the dorsal pallidum and subthalamic nucleus. *J. Neurosci.* **40**, 2859–2867 (2020).
 76. Johnson, L. A. et al. High-frequency oscillations in the pallidum: a pathophysiological biomarker in Parkinson's disease?. *Mov. Disord.* **36**, 1332–1341 (2021).
 77. Scherer, M. et al. Single-neuron bursts encode pathological oscillations in subcortical nuclei of patients with Parkinson's disease and essential tremor. *Proc. Natl. Acad. Sci. USA* **119**, e2205881119 (2022).
 78. Sumarac, S. et al. Interrogating basal ganglia circuit function in Parkinson's disease and dystonia. *eLife* <https://doi.org/10.7554/eLife.90454> (2023).
 79. Ellens, D. J. & Leventhal, D. K. Review: electrophysiology of basal ganglia and cortex in models of Parkinson disease. *J. Park. Dis.* **3**, 241–254 (2013).
 80. Tachibana, Y., Iwamuro, H., Kita, H., Takada, M. & Nambu, A. Subthalamo-pallidal interactions underlying parkinsonian neuronal oscillations in the primate basal ganglia. *Eur. J. Neurosci.* **34**, 1470–1484 (2011).
 81. Raz, A., Vaadia, E. & Bergman, H. Firing patterns and correlations of spontaneous discharge of pallidal neurons in the normal and the tremulous 1-methyl-4-phenyl-1,2,3,6-tetrahydropyridine vervet model of parkinsonism. *J. Neurosci.* **20**, 8559–8571 (2000).
 82. Leblois, A. et al. Late emergence of synchronized oscillatory activity in the pallidum during progressive Parkinsonism. *Eur. J. Neurosci.* **26**, 1701–1713 (2007).
 83. Hahn, P. J. et al. Pallidal burst activity during therapeutic deep brain stimulation. *Exp. Neurol.* **211**, 243–251 (2008).
 84. Lankarany, M., Al-Basha, D., Ratté, S. & Prescott, S. A. Differentially synchronized spiking enables multiplexed neural coding. *Proc. Natl. Acad. Sci. USA* **116**, 10097–10102 (2019).
 85. Caruso, V. C. et al. Single neurons may encode simultaneous stimuli by switching between activity patterns. *Nat. Commun.* **9**, 2715 (2018).
 86. Rodriguez, M. C. et al. The subthalamic nucleus and tremor in Parkinson's disease. *Mov. Disord.* **13**, 111–118 (1998).
 87. Rodriguez-Oroz, M. C. et al. The subthalamic nucleus in Parkinson's disease: somatotopic organization and physiological characteristics. *Brain J. Neurol.* **124**, 1777–1790 (2001).
 88. Asch, N. et al. Independently together: subthalamic theta and beta opposite roles in predicting Parkinson's tremor. *Brain Commun* **2**, fcaa074 (2020).
 89. Magnin, M., Morel, A. & Jeanmonod, D. Single-unit analysis of the pallidum, thalamus and subthalamic nucleus in parkinsonian patients. *Neuroscience* **96**, 549–564 (2000).
 90. Neumann, W.-J. & Kühn, A. A. Subthalamic beta power—unified Parkinson's disease rating scale III correlations require akinetic symptoms. *Mov. Disord.* **32**, 175–176 (2017).
 91. Beudel, M. et al. Oscillatory beta power correlates with akinesia-rigidity in the Parkinsonian subthalamic nucleus. *Mov. Disord.* **32**, 174–175 (2017).
 92. Weinberger, M. et al. Beta oscillatory activity in the subthalamic nucleus and its relation to dopaminergic response in Parkinson's disease. *J. Neurophysiol.* **96**, 3248–3256 (2006).
 93. Kühn, A. A., Kupsch, A., Schneider, G.-H. & Brown, P. Reduction in subthalamic 8–35 Hz oscillatory activity correlates with clinical improvement in Parkinson's disease. *Eur. J. Neurosci.* **23**, 1956–1960 (2006).
 94. Tinkhauser, G. et al. The modulatory effect of adaptive deep brain stimulation on beta bursts in Parkinson's disease. *Brain J. Neurol.* **140**, 1053–1067 (2017).
 95. Fim Neto, A. et al. Subthalamic low beta bursts differ in Parkinson's disease phenotypes. *Clin. Neurophysiol.* **140**, 45–58 (2022).
 96. Guo, S. et al. Neuronal firing patterns in the subthalamic nucleus in patients with akinetic-rigid-type Parkinson's disease. *J. Clin. Neurosci.* **19**, 1404–1407 (2012).
 97. Wang, D. D. et al. Pallidal deep-brain stimulation disrupts pallidal beta oscillations and coherence with primary motor cortex in Parkinson's disease. *J. Neurosci.* **38**, 4556–4568 (2018).
 98. Piña-Fuentes, D. et al. Adaptive DBS in a Parkinson's patient with chronically implanted DBS: a proof of principle. *Mov. Disord.* **32**, 1253–1254 (2017).
 99. Piña-Fuentes, D. et al. The characteristics of pallidal low-frequency and beta bursts could help implementing adaptive brain stimulation in the Parkinsonian and dystonic internal globus pallidus. *Neurobiol. Dis.* **121**, 47–57 (2019).
 100. Darcy, N. et al. Spectral and spatial distribution of subthalamic beta peak activity in Parkinson's disease patients. *Exp. Neurol.* **356**, 114150 (2022).
 101. Logothetis, N. K., Pauls, J., Augath, M., Trinath, T. & Oeltermann, A. Neurophysiological investigation of the basis of the fMRI signal. *Nature* **412**, 150–157 (2001).
 102. Connolly, A. T. et al. Modulations in oscillatory frequency and coupling in globus pallidus with increasing Parkinsonian severity. *J. Neurosci.* **35**, 6231–6240 (2015).
 103. Al-Ozzi, T. M., Botero-Posada, L. F., Lopez Rios, A. L. & Hutchison, W. D. Single unit and beta oscillatory activities in subthalamic nucleus are modulated during visual choice preference. *Eur. J. Neurosci.* **53**, 2220–2233 (2021).
 104. Milosevic, L. et al. Online mapping with the deep brain stimulation lead: a novel targeting tool in Parkinson's disease. *Mov. Disord.* **35**, 1574–1586 (2020).
 105. Tinkhauser, G. et al. Directional local field potentials: a tool to optimize deep brain stimulation. *Mov. Disord.* **33**, 159–164 (2018).
 106. Wong, J. K. et al. STN versus GPi deep brain stimulation for action and rest tremor in Parkinson's disease. *Front. Hum. Neurosci.* **14**, 578615 (2020).
 107. Zeng, Z. et al. Effects of unilateral stimulation in Parkinson's disease: a randomized double-blind crossover trial. *Front. Neurol.* **12**, 812455 (2022).
 108. Mei, S. et al. Three-year gait and axial outcomes of bilateral STN and GPi Parkinson's disease deep brain stimulation. *Front. Hum. Neurosci.* **14**, 1 (2020).
 109. George, R. J. S., Nutt, J. G., Burchiel, K. J. & Horak, F. B. A meta-regression of the long-term effects of deep brain stimulation on balance and gait in PD. *Neurology* **75**, 1292–1299 (2010).
 110. Fasano, A., Aquino, C. C., Krauss, J. K., Honey, C. R. & Bloem, B. R. Axial disability and deep brain stimulation in patients with Parkinson disease. *Nat. Rev. Neurol.* **11**, 98–110 (2015).
 111. Foffani, G. & Alegre, M. Chapter 18—Brain oscillations and Parkinson disease. In *Handbook of Clinical Neurology* (eds Quartarone, A. et al.) Vol. 184, 259–271 (Elsevier, 2022).
 112. Ray, S. & Maunsell, J. H. R. Different origins of gamma rhythm and high-gamma activity in macaque visual cortex. *PLoS Biol.* **9**, e1000610 (2011).
 113. Pardo-Valencia, J., Fernández-García, C., Alonso-Frech, F. & Foffani, G. Oscillatory vs. non-oscillatory subthalamic beta activity in Parkinson's disease. *J. Physiol.* **602**, 373–395 (2024).
 114. Hutchison, W. D. et al. Neurophysiological identification of the subthalamic nucleus in surgery for Parkinson's disease. *Ann. Neurol.* **44**, 622–628 (1998).
 115. Rey, H. G., Pedreira, C. & Quiñero, R. Past, present and future of spike sorting techniques. *Brain Res. Bull.* **119**, 106–117 (2015).

116. Arachchige, C. N. P. G., Prendergast, L. A. & Staudte, R. G. Robust analogs to the coefficient of variation. *J. Appl. Stat.* **49**, 268–290 (2022).
117. Kaneoke, Y. & Vitek, J. L. Burst and oscillation as disparate neuronal properties. *J. Neurosci. Methods* **68**, 211–223 (1996).
118. Anderson, R. W. et al. A novel method for calculating beta band burst durations in Parkinson's disease using a physiological baseline. *J. Neurosci. Methods* **343**, 108811 (2020).
119. Moran, A., Bergman, H., Israel, Z. & Bar-Gad, I. Subthalamic nucleus functional organization revealed by Parkinsonian neuronal oscillations and synchrony. *Brain J. Neurol.* **131**, 3395–3409 (2008).
120. Kehnemouyi, Y. M. et al. Modulation of beta bursts in subthalamic sensorimotor circuits predicts improvement in bradykinesia. *Brain J. Neurol.* **144**, 473–486 (2021).

Acknowledgements

The authors would like to thank the participants for their contributions to the work. This project has been made possible with the financial support of Health Canada, through the Canada Brain Research Fund, an innovative partnership between the Government of Canada (through Health Canada) and Brain Canada, and of the Azrieli Foundation (L.M.); Natural Sciences and Engineering Council (NSERC) RGPIN-2022-05181 (L.M.); Parkinson Canada (S.S.; L.M.). The funders played no role in study design, data collection, analysis and interpretation of data, or the writing of this manuscript.

Author contributions

(1) Research project: A. Conception, B. Organization, C. Execution; (2) Statistical analysis: A. Design, B. Execution, C. Review and critique; (3) Manuscript preparation: A. Writing of the first draft, B. Review and critique. S.S.: 1B, 1C, 2A, 2B and 3A; J.Y.: 1B and 3B; C.F.: 1B and 3B; L.Z.: 1B and 3B; P.K.: 1B and 3B; O.F.: 1B and 3B; M.P.: 1B and 3B; M.H.: 1B and 3B; S.K.: 1B and 3B; A.L.: 1B and 3B; W.H.: 1B and 3B; A.F.: 1B and 3B; L.M.: 1A, 1B, 2A, 2C, and 3B.

Competing interests

The authors declare no competing interests.

Additional information

Supplementary information The online version contains supplementary material available at <https://doi.org/10.1038/s41531-024-00773-4>.

Correspondence and requests for materials should be addressed to Luka Milosevic.

Reprints and permissions information is available at <http://www.nature.com/reprints>

Publisher's note Springer Nature remains neutral with regard to jurisdictional claims in published maps and institutional affiliations.

Open Access This article is licensed under a Creative Commons Attribution-NonCommercial-NoDerivatives 4.0 International License, which permits any non-commercial use, sharing, distribution and reproduction in any medium or format, as long as you give appropriate credit to the original author(s) and the source, provide a link to the Creative Commons licence, and indicate if you modified the licensed material. You do not have permission under this licence to share adapted material derived from this article or parts of it. The images or other third party material in this article are included in the article's Creative Commons licence, unless indicated otherwise in a credit line to the material. If material is not included in the article's Creative Commons licence and your intended use is not permitted by statutory regulation or exceeds the permitted use, you will need to obtain permission directly from the copyright holder. To view a copy of this licence, visit <http://creativecommons.org/licenses/by-nc-nd/4.0/>.

© The Author(s) 2024